PCCP

ROYAL SOCIETY OF CHEMISTRY

PAPER

View Article Online
View Journal | View Issue

Check for updates

Cite this: *Phys. Chem. Chem. Phys.*, 2022, **24**, 8233

Magnetic and magnetocaloric effect study of a polycrystalline $Gd_{0.5}Sr_{0.5-x}Ca_xMnO_3$ compound†

Soma Chatterjee,[a] Kalipada Das *[b] and I. Das[a]

Received 8th January 2022,
Accepted 7th March 2022

DOI: 10.1039/d2cp00114d

rsc.li/pccp

The magnetic and magnetocaloric properties of polycrystalline $Gd_{0.5}Sr_{0.5-x}Ca_xMnO_3$ (x = 0.0, 0.2, 0.3, 0.4 and 0.5) compounds have been investigated. Depending upon the Ca and Sr proportions, fascinating magnetic ground states were observed in the $Gd_{0.5}Sr_{0.5-x}Ca_xMnO_3$ compounds. Here, the dominating nature of the canted magnetic state (for the $Gd_{0.5}Ca_{0.5}MnO_3$ compound) and glassy (disordered ferromagnetic) magnetic state (for the $Gd_{0.5}Sr_{0.5}MnO_3$ compound) are observed. However, for the intermediate doped samples (x = 0.2, 0.3, 0.4), a competing nature is found in their magnetic and exchange bias properties. Additionally, in the low temperature region, a significantly large magnetocaloric effect is observed for all the samples. At a 70 kOe external magnetic field, the highest observed value of the magnetocaloric entropy change is 21.58 J kg^{-1} K^{-1} (for the $Gd_{0.5}Ca_{0.5}MnO_3$ sample) and the lowest is 10.15 J kg^{-1} K^{-1} (for the $Gd_{0.5}Sr_{0.5}MnO_3$ sample).

Published on 23 March 2022. Downloaded by Indian Institute of Technology Kanpur on 4/11/2022 7:21:08 AM.

1 Introduction

Extensive research work has been performed on doped perovskite manganites in the last three decades.[1,2] Generally, perovskite manganites are represented by the formula $LnMnO_3$ (where 'Ln' is the trivalent rare earth element). In $LnMnO_3$type compounds, the Mn ion has the fixed valence state (+3). In the low temperature region, such undoped perovskite manganites exhibit an electrically insulating and magnetically antiferromagnetic (A-type) nature.[3] In contrast to this, several appealing physical properties appear when the trivalent site is partially doped by bivalent ions with the valence state (+2). Due to the doping of bivalent ions, the same percentage of Mn^{3+} ions will be converted into Mn^{4+} ions, which gives rise to several fascinating properties in doped perovskite manganites.[4–6] Ferromagnetism, charge ordering, colossal magnetoresistance effect (CMR), large magnetocaloric effect (MCE) *etc.* are very well documented properties of doped perovskite manganites.[7–13] These properties in several type of doped perovskite manganite compounds having different compositions have been extensively studied.[14–22] In addition to this, the crystal structure, magnetic properties and electrical properties are well connected to each other in these compounds.[17,18,22–32] As a result of doping, the crystal structure of the compound will also get modified depending upon the size mismatch of the trivalent and bivalent ions, which influences the physical properties significantly.[33,34] Near to a fifty percent doping concentration of bivalent ions, doped manganite generally exhibits the real space ordering of Mn^{3+} and Mn^{4+} ions. Such regular ordering of Mn^{3+} and Mn^{4+} ions in a crystal is known as charge ordering. This phenomenon is almost a generic nature of doped manganite systems. Charge ordering is often accompanied by an anti-ferromagnetic transition upon reduction of the temperature. However, there are some cases in which a clear antiferromagnetic signature is not present even below the charge ordering transition temperature.[35] The substitution of a large cation by a smaller cation will change the unit cell dimensions and orbital overlapping. The stability of charge ordering also depends on the cation size because orbital overlapping is an important factor in charge ordering.[36–38]

To elucidate the magnetic ground state of any magnetic material, the magnetocaloric effect may be treated as a powerful tool.[39–41] The magnetocaloric effect (MCE) is defined by the isothermal magnetic entropy change or adiabatic temperature change of a magnetic material when it is subjected to an external magnetic field. It has been reported that any feeble magnetic transition can be easily detected by the magnetocaloric effect due to its more sensitive nature. Moreover, besides these fundamental aspects, the magnetocaloric effect is also important from a technological aspect.[42–52] In contrast to cryogenic gas compression cooling technology, the use of solid-state refrigerant materials is more beneficial for environmentally friendly cooling technology based on the magnetocaloric effect (MCE). To select a solid-state material as a suitable refrigerant, the magnetocaloric response should be significantly large. Materials having a large MCE at the cryogenic region and room temperature region are

[a] *CMP Division, Saha Institute of Nuclear Physics, HBNI, AF-Bidhannagar, Kolakta, 700064, India*
[b] *Department of Physics, Seth Anandram Jaipuria College, 10-Raja Nabakrishna Street, Kolkata, 700005, India. E-mail: kalipadadasphysics@gmail.com*

† PACS: 75.47.Lx, 73.63.Bd.

Published on 23 March 2022. Downloaded by Indian Institute of Technology Kanpur on 4/11/2022 7:21:08 AM.

important as suitable refrigerant materials from a technological perspective. Searching for promising refrigerant materials with large MCEs is an important question in current research. Regarding this context, perovskite manganite compounds have also received considerable interest as intermetallic compounds due to several beneficial aspects, such as their insulating nature, high chemical stability, cheap commercial cost *etc.* It has been well documented in several studies that a large magnetocaloric effect is observed in compounds with large magnetic moments. Initially, Gd and several Gd based intermetallic compounds were treated as promising magnetocaloric materials due to their large magnetic moments.[53,54] Similarly, many doped manganite samples also show large MCEs due to their long-range magnetic ordering and large magnetization values.[55] Additionally, the magnetocaloric effect is also influenced by the ground state magnetic configuration. As context for this, the short-range effect mediated large MCEs of Ho_5Pd_2 and some manganite samples have been previously reported.[56] To identify magnetic refrigerant materials with large MCEs, the relative cooling power (RCP) or refrigerant capacity (RC) are other important parameters. To calculate the RCP/RC, the span of the temperature at half of the value of the magnetic entropy change ($-\Delta S$) is required.[57]

Systematic studies about the influence of the glassy state and canted anti-ferromagnetic state on the MCE are rarely found. To serve this purpose, we have selected a series of polycrystalline manganite compounds $Gd_{0.5}Sr_{0.5-x}Ca_xMnO_3$ (x = 0.0, 0.2, 0.3, 0.4, 0.5). In this series, the magnetic ground state of the end members are glassy and canted type, respectively.[58,59] As reported earlier, $Gd_{0.5}Sr_{0.5}MnO_3$ possesses a charge ordering transition at T = 95 K and a cluster glass transition near a temperature of 42 K.[58,59] However, the $Gd_{0.5}Ca_{0.5}MnO_3$ compound exhibits a charge ordering transition at 300 K and a canted magnetic state is found near a temperature of 150 K.[50,60] The aim of the present study is to examine the effect of the competing nature of different ground states in $Gd_{0.5}Sr_{0.5-x}Ca_xMnO_3$ (x = 0.0, 0.2, 0.3, 0.4,0.5) compounds and correlate this with their structural properties. Our experimental results indicate that with the modification of the magnetic ground state, the MCE properties of the compound are influenced markedly. Additionally, the numerical value of the magnetic entropy change at low temperature get importance on its magnetic configuration.

2 Sample preparation, characterizations and measurements

Polycrystalline $Gd_{0.5}Sr_{0.5-x}Ca_xMnO_3$ (x = 0.0, 0.2, 0.3, 0.4, 0.5) compounds were synthesized by a conventional sol–gel method. Highly pure Gd_2O_3 (99.99%), $CaCO_3$ (99.99%), $SrCO_3$ (99.99%) and MnO_2 (99.9%) (from Alfa Aesar) were used as the starting elements for sample preparation. At the first stage of the sample preparation, the required amounts of deionized water and nitric acid were added with stoichiometric primary components to get a clear solution. The clear solution for MnO_2 was obtained after adding suitable amount of oxalic acid. Then, all the homogeneous solutions were mixed up by a magnetic stirrer and an appropriate amount of citric acid was added to it. The chemical reactions during sol–gel conversion can be described by the following equation:

$$(0.25)Gd_2O_3 + (0.5 - x)SrCO_3 + (x)CaCO_3 + HNO_3 + H_2O + \text{oxalic acid} + \text{citric acid} \rightarrow Gd_{0.5}Sr_{0.5-x}Ca_xMnO_3 + CO_2 + NO_2 + N_2 + H_2O$$

By using a water bath, the solution was heated at 80–90 °C until a gel was formed. Then, the gel was decomposed at a higher temperature and, finally, a black powder was formed. After pelletizing the powder, all the compounds were heat treated for the synthesis of bulk compound at 1300 °C for 36 hours.

It is well known that oxygen plays a crucial role in determining the physical properties of perovskite oxide materials and oxygen non-stoichiometry can influence the physical properties of the compounds.[61,62] Magnetic interaction and electron conduction can be significantly modified due to the presence of oxygen vacancies. Such changes are usually manifested in transitions. In the present case, there is no significant change in transition temperatures in comparison to the previously reported articles of the end compounds. We have observed that all three transitions – glassy type, charge ordering and canted antiferromagnetic – are in good agreement with other articles.[50,58–60] Hence, it may be assumed that oxygen non-stoichiometry is not significant in this case.

Room temperature powder X-ray diffraction study was done by a Rigaku TTRAX-III diffractometer using Cu-K_α radiation (λ = 1.54 Å). To study the surface morphology and elemental analysis of all compounds, field emission scanning electron microscopy (FESEM) and energy dispersive X-ray analysis (EDXA) measurements were performed. Magnetic measurements were carried out by a super conducting quantum interference device (SQUID-VSM) magnetometer.

3 Results and discussion

Room temperature X-ray diffraction studies indicate the single-phase nature of all the compounds. Structural modelling of the X-ray diffraction data was performed by using fullprof software. Rietveld refinement was carried out to estimate the lattice parameters and atomic positions of Gd, Sr and Ca (*i.e.* Wyckoff positions, sites with constant occupancy) for all the studied compounds. The X-ray diffraction patterns, along with the Rietveld fitting of all samples, are displayed in Fig. 1(a–e). The unit cell volume gradually decreased from the $Gd_{0.5}Sr_{0.5}MnO_3$ compound to the $Gd_{0.5}Ca_{0.5}MnO_3$ compound (shown in the inset of Fig. 1(f)). The Mn–Mn bond length and Mn–O–Mn bond angle are extracted by using Vesta software. The extracted lattice parameters, atomic positions, bond lengths and bond angles are listed in Table 1. The structural parameters match quite well to those reported previously.[63]

For the $Gd_{0.5}Sr_{0.5}MnO_3$ compound, the extracted lattice parameters indicate that $a \sim c < b$. Gradual distortion from

 This journal is © the Owner Societies 2022

Published on 23 March 2022. Downloaded by Indian Institute of Technology Kanpur on 4/11/2022 7:21:08 AM.

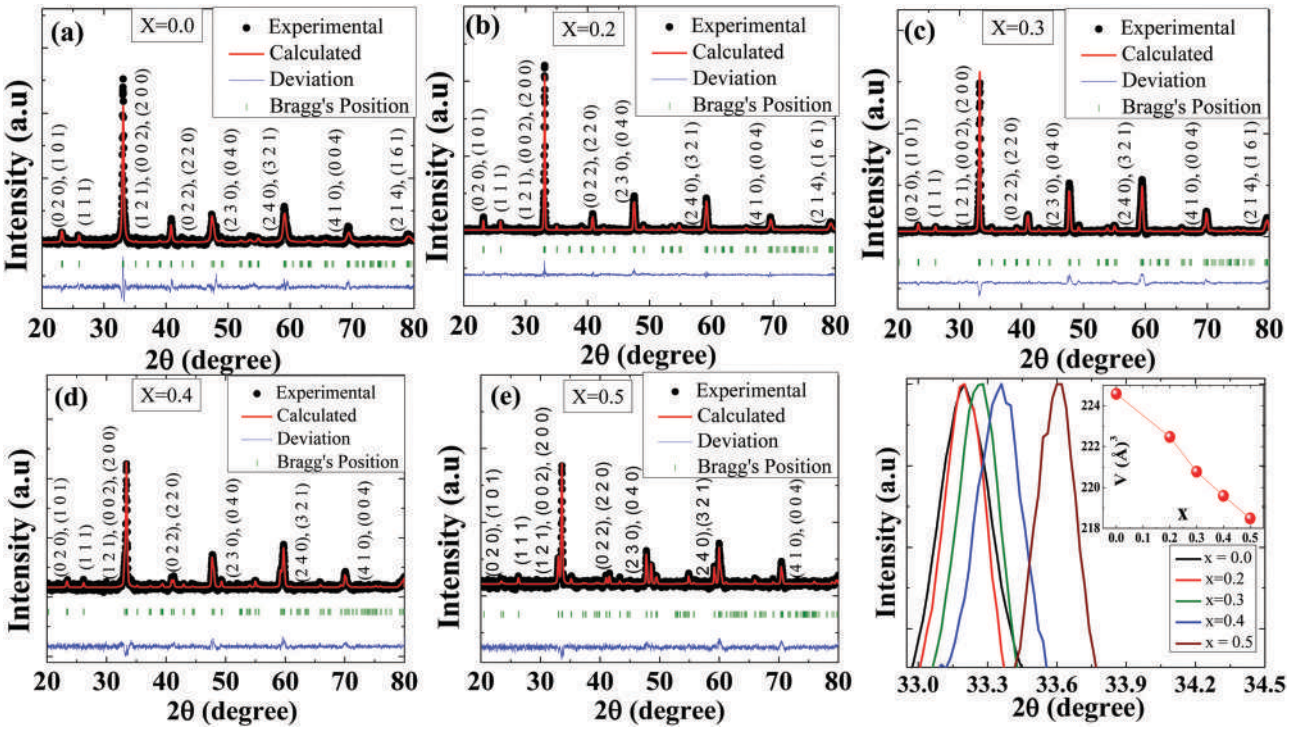

Fig. 1 (a)–(e) Room temperature X-ray diffraction patterns of all studied compounds. The red colored line in each panel indicates the fitted data. (f) The enlarged view of the maximum intense Bragg peak of the X-ray diffraction data and the inset of (f) shows the variation of the unit cell volume with the doping concentration x for the $Gd_{0.5}Sr_{0.5-x}Ca_xMnO_3$ (x = 0.0, 0.2, 0.3, 0.4 and 0.5) compounds.

a pseudo cubic structure was observed for the x = 0.0 to 0.4 compounds (the a side length is nearly constant, and the b and c side lengths decrease regularly). However, for the $Gd_{0.5}Ca_{0.5}MnO_3$ compound, a rapid change in the lattice parameters was observed

Table 1 Structural parameters for the $Gd_{0.5}Sr_{0.5-x}Ca_xMnO_3$ (x = 0.0, 0.2, 0.3, 0.4 and 0.5) compounds

			Wyckoff position (with occ.)									
Sample	Component	Site	x	y	z	Occ.	a (Å)	b (Å)	c (Å)	V (Å)^3	Mn–Mn	Mn–O–Mn
$Gd_{0.5}Sr_{0.5}MnO_3$	Gd	4c	0.4885	0.2500	0.0046	0.2500	5.4268	7.6276	5.4255	224.5802	3.81213 Å	159.79°
	Sr	4c	0.4885	0.2500	0.0046	0.2500	(±0.0008)	(±0.0008)	(±0.0008)			
	Mn	4a	0.0000	0.0000	0.0000	0.5000						
	O1	8d	0.2329	0.0446	0.2361	1.0000						
	O2	4c	0.5571	0.2500	0.4996	0.5067						
$Gd_{0.5}Sr_{0.3}Ca_{0.2}MnO_3$	Gd	4c	0.4760	0.2500	0.0133	0.2500	5.4133	7.6215	5.3920	222.5165	3.8091 Å	163.70°
	Sr	4c	0.4760	0.2500	0.0133	0.2500	(±0.0005)	(±0.0007)	(±0.0006)			
	Ca	4c	0.4760	0.2500	0.0133	0.2500						
	Mn	4a	0.0000	0.0000	0.0000	0.5000						
	O1	8d	0.2187	0.0188	0.2800	1.0000						
	O2	4c	0.5359	0.2500	0.6080	0.5000						
$Gd_{0.5}Sr_{0.2}Ca_{0.3}MnO_3$	Gd	4c	0.4696	0.2500	0.0041	0.2500	5.4085	7.5953	5.3744	220.78	3.7976 Å	161.38°
	Sr	4c	0.4696	0.2500	0.0041	0.2500	(±0.0003)	(±0.0005)	(±0.0003)			
	Ca	4c	0.4696	0.2500	0.0041	0.2500						
	Mn	4a	0.0000	0.0000	0.0000	0.5000						
	O1	8d	0.2273	0.3320	0.2757	1.0000						
	O2	4c	0.5240	0.2500	0.5844	0.5000						
$Gd_{0.5}Sr_{0.1}Ca_{0.4}MnO_3$	Gd	4c	0.4641	0.2500	0.0024	0.2500	5.4153	7.5735	5.3541	219.5910	3.7868 Å	147.42°
	Sr	4c	0.4641	0.2500	0.0024	0.2500	(±0.0006)	(±0.0009)	(±0.0005)			
	Ca	4c	0.4641	0.2500	0.0024	0.2500						
	Mn	4a	0.0000	0.0000	0.0000	0.5000						
	O1	8d	0.1984	0.0506	0.3043	1.0000						
	O2	4c	0.5328	0.2500	0.6005	0.5000						
$Gd_{0.5}Ca_{0.5}MnO_3$	Gd	4c	0.4559	0.2500	0.0018	0.2500	5.4449	7.5097	5.3434	218.4894	3.7548 Å	149.99°
	Ca	4c	0.4559	0.2500	0.0018	0.2500	(±0.0004)	(±0.0007)	(±0.0004)			
	Mn	4a	0.0000	0.0000	0.0000	0.5000						
	O1	8d	0.1842	0.0265	0.3075	1.0000						
	O2	4c	0.5033	0.2500	0.5906	0.5000						

Published on 23 March 2022. Downloaded by Indian Institute of Technology Kanpur on 4/11/2022 7:21:08 AM.

(the a side increases and c side reduces) and the reflections were indexed as an orthorhombic ($c < a < b$) structure (from Table 1), similar to that reported previously.[64] The sudden structural change from $Gd_{0.5}Sr_{0.1}Ca_{0.4}MnO_3$ to $Gd_{0.5}Ca_{0.5}MnO_3$ was also observed directly from the experimental X-ray diffraction data (shown in Fig. 1f). The main peak of normalized intensity is observed at different values of 2θ and the difference is comparatively larger for $Gd_{0.5}Ca_{0.5}MnO_3$ than the compounds with other Sr contents. The substitution of the Sr^{2+} ion by the smaller cation Ca^{2+} will change the unit cell volume, as well as orbital overlapping. The Mn–Mn bond length decreases from x = 0.0 (GSMO) to 0.5 (GCMO). So, orbital overlapping increases, which corresponds to the increase of the charge order stability. The Mn–O–Mn bond angle decreases from GSMO to GCMO, which decreases the bandwidth.[36] This structural effect can stabilize the charge ordered and orbital ordered states for the GCMO compound over the GSMO compound.

Local structural measurements, such as energy dispersive X-ray analysis (EDXA) with scanning electron microscopy imaging, were performed for elemental data analysis by using a field emission scanning electron microscope (and are shown in Fig. 2). Table 2 shows that the atomic percentage of each component of a particular compound nicely matches with the chemical composition of that compound.

From Table 3, we observe that the value of the grain size (from scanning electron microscopy) is much larger than the crystallite size (calculated from XRD analysis). This indicates that each particle consists of many crystallites. Particle size/crystallite size is an important tool for controlling the magnetic and magnetocaloric properties of compounds. Interestingly, the magnetization and magnetocaloric effect are directly influenced by the reduction of the particle size. The values of magnetization, Curie temperature and magnetocaloric entropy change decrease with the reduction of the crystallite size[65].

The magnetization as a function of temperature of all compounds has been measured using three different protocols.

Zero field cooled warming (ZFCW): in this protocol, samples were first cooled down in the absence of an external magnetic field down to the lowest temperature (5 K in this present study). Then, a constant magnetic field was applied and magnetization data were collected during warming from 5 K to 300 K (rate of 5 K min^{-1}).

Field cooled cooling (FCC): to measure the magnetization in this protocol, a magnetic field was applied at room temperature

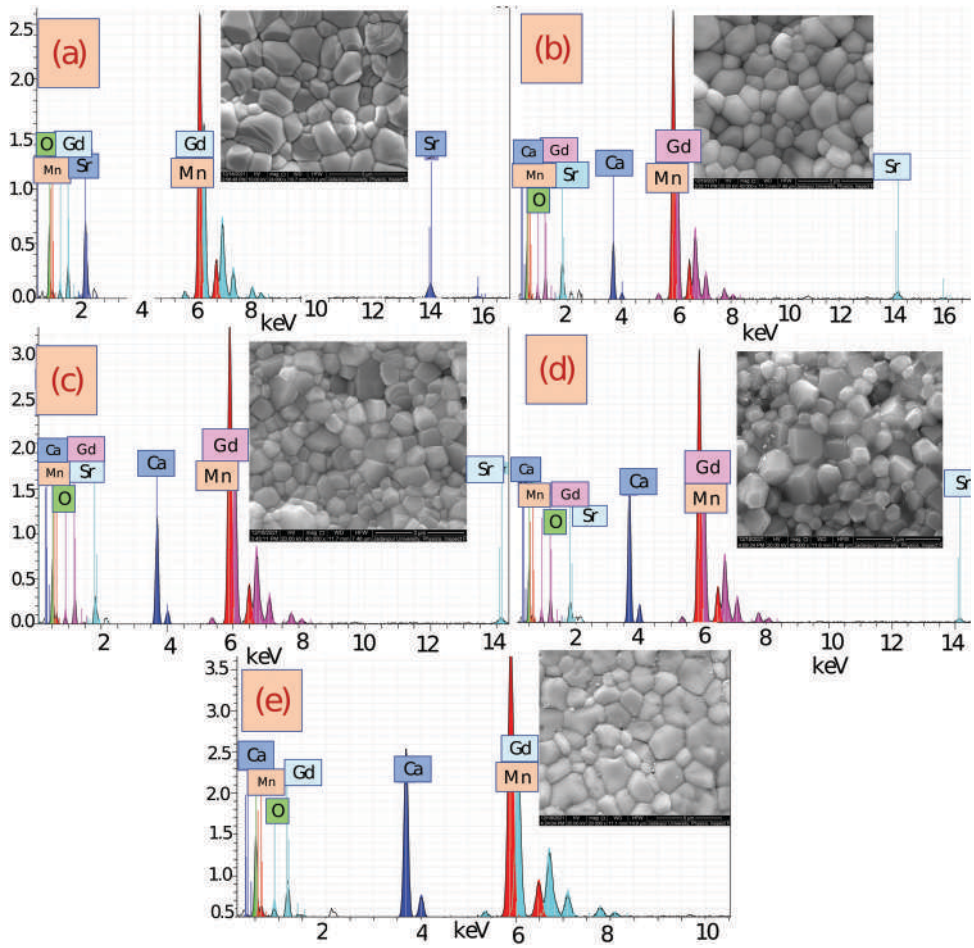

Fig. 2 (a)–(e) Energy dispersive X-ray analysis (EDXA), with the scanning electron microscopy images in the inset of all figures, for the $Gd_{0.5}Sr_{0.5-x}Ca_xMnO_3$ (x = 0.0, 0.2, 0.3, 0.4 and 0.5) compounds.

 This journal is © the Owner Societies 2022

Published on 23 March 2022. Downloaded by Indian Institute of Technology Kanpur on 4/11/2022 7:21:08 AM.

Table 2 Atomic percentages of elemental composition (from EDXA) of the $Gd_{0.5}Sr_{0.5-x}Ca_xMnO_3$ (x = 0.0, 0.2, 0.3, 0.4 and 0.5) compounds

Compound	Gd (at%)	Sr (at%)	Ca (at%)	Mn (at%)	O (at%)
$Gd_{0.5}Sr_{0.5}MnO_3$	11.90	13.04	0.00	22.08	52.97
$Gd_{0.5}Sr_{0.3}Ca_{0.2}MnO_3$	11.50	7.41	4.50	23.72	52.88
$Gd_{0.5}Sr_{0.2}Ca_{0.3}MnO_3$	11.32	5.48	7.10	23.27	52.83
$Gd_{0.5}Sr_{0.1}Ca_{0.4}MnO_3$	10.92	3.41	10.06	22.87	52.73
$Gd_{0.5}Ca_{0.5}MnO_3$	11.19	0.00	12.02	24.00	52.80

Table 3 Crystallite size and particle size for $Gd_{0.5}Sr_{0.5-x}Ca_xMnO_3$ (x = 0.0, 0.2, 0.3, 0.4 and 0.5) compounds

Compound	Crystallite size from XRD (in nm)	Particle size from SEM (in μm)
$Gd_{0.5}Sr_{0.5}MnO_3$	64.63	1.39
$Gd_{0.5}Sr_{0.3}Ca_{0.2}MnO_3$	92.12	1.11
$Gd_{0.5}Sr_{0.2}Ca_{0.3}MnO_3$	57.29	1.23
$Gd_{0.5}Sr_{0.1}Ca_{0.4}MnO_3$	57.41	1.01
$Gd_{0.5}Ca_{0.5}MnO_3$	66.02	1.38

(300 K) and the temperature dependent magnetization was recorded during cooling from 300 K to 5 K.

Field cooled warming (FCW): after the FCC magnetization measurement, the sample was again warmed with the same magnetic field and the magnetization *vs.* temperature data was recorded during the warming cycle (5K to 300 K).

The temperature dependent magnetization of the $Gd_{0.5}Sr_{0.5-x}Ca_xMnO_3$ (x = 0.0, 0.2, 0.3, 0.4, 0.5) series of compounds is shown in Fig. 3(a–e) at H = 500 Oe and the variation of the maximum magnetization value with the doping concentration (x) is shown in Fig. 3(f). The steeper increase of magnetization in Fig. 3(a) demonstrates the charge ordering (CO) transition ($T \sim 95$ K) and cluster glass (CG) like transition ($T \sim 42$ K) for the $Gd_{0.5}Sr_{0.5}MnO_3$ (GSMO) compound, similar to that reported previously.[58,59] On the other hand, it has already been reported that the $Gd_{0.5}Ca_{0.5}MnO_3$ (GCMO) compound shows a charge ordering (CO) transition ($T \sim 300$ K) and canted antiferromagnetic (CAFM) transition ($T \sim 150$ K), which is shown in Fig. 3(e).[50,60,66] So, a smooth crossover from the glassy transition (x = 0.0) to canted AFM transition (x = 0.5) may be observed for the mixture of Sr and Ca doped intermediate components (x = 0.2, 0.3, 0.4). However, the charge ordering transition is not clearly detected for x = 0.2, 0.3, 0.4 compounds (shown in Fig. 3(b–d)) from the 'dc' magnetization data. The strength of the glassy type transition (nearly at the same temperature of $T \sim 42$ K) is smoothly reduced from x = 0.2 to x = 0.4. Fig. 3(d) shows that the glassy transition becomes very feeble for x = 0.4 and it totally vanishes for x = 0.5 (Fig. 3(e)). The reduction of the saturation magnetization with increasing Ca concentration may be addressed by considering the reduction of the electronic bandwidth of the sample due to the smaller ionic radius of the Ca ion. The derivative of magnetization with temperature for all the compounds is calculated and the transition temperature (T_C) can be determined from the lowest value of dM/dT. In our present study, the dM/dT *vs.* T curve shows $T_C \sim 44$ K for the x = 0.0–0.4 compounds, which corresponds to the glassy (disordered ferro)

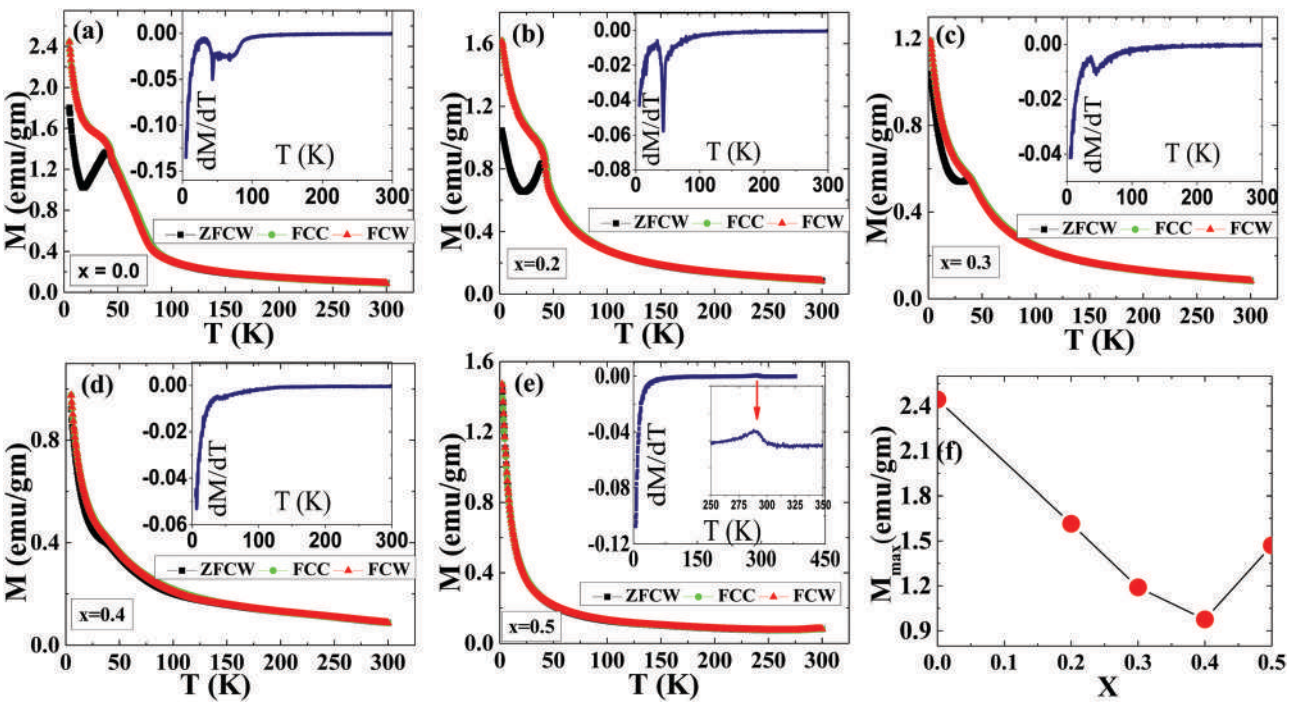

Fig. 3 Temperature dependence of magnetization for $Gd_{0.5}Sr_{0.5-x}Ca_xMnO_3$ in the ZFCW, FCC and FCW modes at H = 500 Oe with (a) x = 0.0, (b) x = 0.2, (c) x = 0.3, (d) x = 0.4 and (e) x = 0.5, and (f) shows the variation of the maximum value of magnetization with the doping concentration x for $Gd_{0.5}Sr_{0.5-x}Ca_xMnO_3$ (x = 0.0, 0.2, 0.3, 0.4 and 0.5) compounds. The insets of (a–e) show the derivative of magnetization (dM/dT) *vs.* temperature.

Published on 23 March 2022. Downloaded by Indian Institute of Technology Kanpur on 4/11/2022 7:21:08 AM.

type transition. Although the T_C value remains the same, the glassy phase decreases with the doping concentration of Ca and it completely vanishes for the $x = 0.5$ compound (shown in the insets of Fig. 3(a)–(e)). This reason may be due to the decrease of the double exchange interaction (from $x = 0$ to $x = 0.4$) between Mn^{3+} and Mn^{4+} ions. In addition to this, for the $x = 0.5$ sample, a clear peak at $T \sim 300$ K appears (shown in the enlarged view of the inset of Fig. 3(e)), which manifests as a super exchange interaction.

The variation of inverse susceptibility with temperature is plotted in Fig. 4, where different kinds of transitions are clearly observed for all the compounds. Inverse susceptibility follows the Curie–Weiss law at higher temperatures ($T > 200$ K for Fig. 4(a–d) and $T > 300$ K for Fig. 4(e)):

$$\chi = \frac{C}{T - \theta}. \quad (1)$$

The deviation of the experimental data from the fitted straight line may be associated with a transition below a temperature of 200 K.[58] This transition may be expected to be a charge ordering transition because the presence of a CO transition for the end components has already been reported[58] ($T_{CO} \sim 100$ K for $Gd_{0.5}Sr_{0.5}MnO_3$ and $T_{CO} \sim 300$ K for $Gd_{0.5}Ca_{0.5}MnO_3$). Fig. 4(a) shows the presence of cluster glass like transition for the $Gd_{0.5}Sr_{0.5}MnO_3$ compound. Upon increasing the doping concentration of Ca, the glassy transition became feeble. In Fig. 4(d), a very weak glassy transition (at $T \sim 42$ K), as well as an extra new feeble transition (at $T \sim 130$ K), was observed for the $Gd_{0.5}Sr_{0.1}Ca_{0.4}MnO_3$ compound. This new transition may be associated with a canted antiferromagnetic (CAFM) transition because its neighbouring compound $Gd_{0.5}Ca_{0.5}MnO_3$ shows the CAFM transition in the same temperature region. Fig. 4(e) clearly indicates the presence of a CAFM transition ($T_{CAFM} \sim 150$ K) and CO transition ($T_{CO} \sim 300$ K) for the $Gd_{0.5}Ca_{0.5}MnO_3$ compound.[50] Effective magnetic moments (P_{eff}) for all the compounds are calculated from the inverse susceptibility curves. The decreasing nature of P_{eff} with the doping concentration x is shown in Fig. 4(f). The theoretically calculated value of P_{eff} for the Gd based half bivalent doping compound is 7.1424. The experimental value of P_{eff} indicates that a small amount of ferromagnetic clustering may be present for the GSMO compound (P_{eff} (expt) > P_{eff} (calculated)) at the paramagnetic region, although the signature of the Griffith phase (ferromagnetic cluster in the paramagnetic region) is not observed for any of the compounds. The GCMO compound shows a smaller value of P_{eff} because of short-range charge-ordered antiferromagnetic interactions present in the paramagnetic region. This AFM interaction may reduce the value of P_{eff} for GCMO more than the GSMO compound. The competing nature of the field induced ferromagnetic counterpart and inherent glassy disordered phase for $Gd_{0.5}Sr_{0.5}MnO_3$ was elaborately described by Wagh *et al.*[58,59] Previously, Das *et al.* also reported a large value of the MCE for the $Gd_{0.5}Ca_{0.5}MnO_3$ compound in the cryogenic temperature range by considering the magnetic precursor effect of rare-earth ions.[50] Moreover, Nagaraja *et al.* reported a systematic study of the $Gd_{1-x}Sr_xMnO_3$ ($x = 0.2$–0.5) compound and demonstrated its different physical properties with different doping concentrations.[67]

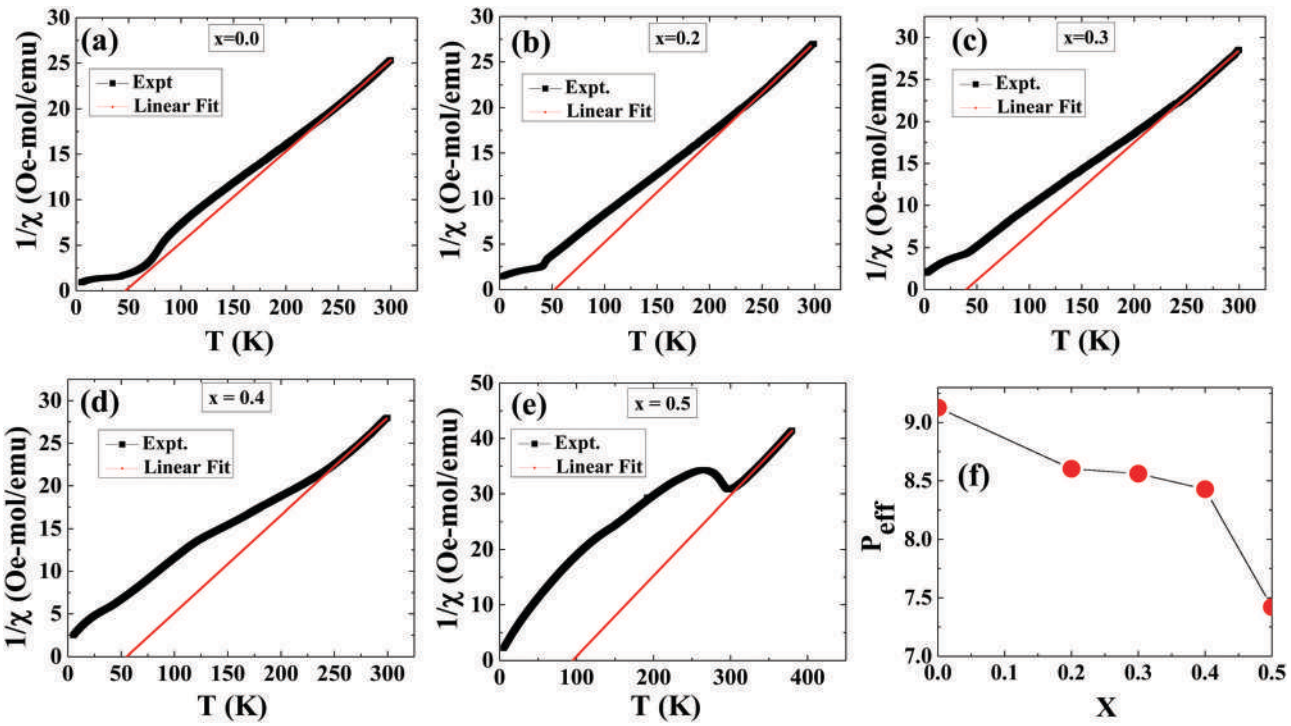

Fig. 4 Variation of inverse susceptibility with temperature and its linear fitting for $Gd_{0.5}Sr_{0.5-x}Ca_xMnO_3$ compounds at $H = 500$ Oe magnetic field with (a) $x = 0.0$, (b) $x = 0.2$, (c) $x = 0.3$, (d) $x = 0.4$ and (e) $x = 0.5$, and (f) shows the variation of the effective magnetic moment with the doping concentration x for the $Gd_{0.5}Sr_{0.5-x}Ca_xMnO_3$ ($x = 0.0$, 0.2, 0.3, 0.4 and 0.5) compounds.

 This journal is © the Owner Societies 2022

Published on 23 March 2022. Downloaded by Indian Institute of Technology Kanpur on 4/11/2022 7:21:08 AM.

The variation of magnetization with temperature at different constant external magnetic fields (H = 500 Oe, 10 kOe, 30 kOe, 50 kOe) for the $Gd_{0.5}Sr_{0.5-x}Ca_xMnO_3$ (x = 0.0, 0.2, 0.3, 0.4, 0.5) compounds are shown in Fig. 5(a–d). Each figure shows that in the low temperature region, the numerical value of magnetization for the GSMO compound is larger than that of the GCMO compound. Low field (H = 500 Oe) M–T data (Fig. 5(a)) clearly shows that the decreasing rate of magnetization is smaller for the GSMO compound compared to the GCMO compound. Hence, we may consider that in the low temperature region, the strength of the interaction between the magnetic ions is stronger for GSMO than those of any other compounds. As the interactions between Gd and Mn ions play a significant role in the low temperature region, a cluster glass like transition appears for the GSMO compound. For the GCMO compound, the Gd ion is in a paramagnetic state even at a low temperature. So, such a cluster glass like transition is not observed for the GCMO compound. For the intermediate doped compounds $Gd_{0.5}Sr_{0.5-x}Ca_xMnO_3$ (x = 0.2, 0.3, 0.4), such glassy behavior is also observed with a decreasing ordered interaction strength (Fig. 5(a)). This glassy behavior disappears for all the compounds at higher constant field values (Fig. 5(b–d)). With increasing magnetic field, Gd and Mn magnetic ions are aligned along the field direction and total magnetization for all compounds in the series increases.

The variation of magnetization with external magnetic field at different constant temperatures for the series of $Gd_{0.5}Sr_{0.5-x}Ca_xMnO_3$ (x = 0.0, 0.2, 0.3, 0.4, 0.5) compounds is shown in Fig. 6. Fig. 6(a) shows the isothermal magnetization for all compounds in the series at T = 2 K. From this figure, it is observed that the maximum value of magnetization decreases in order from x = 0.0 to x = 0.5. The GSMO compound shows a metamagnetic transition (which corresponds to an antiferromagnetic to ferromagnetic transition) at T = 2 K and 20 K (shown in Fig. 5(b)), but when a small amount of Sr is replaced by Ca atoms, the metamagnetic transition disappears (Fig. 6(c)). With increasing the doping concentration of Ca (x = 0.2, 0.3, 0.4, 0.5) the nature of the M–H curve remains same, and only the reduction in magnetization value is observed (Fig. 6(c–f)).

To discuss the magnetocaloric effect for all the $Gd_{0.5}Sr_{0.5-x}Ca_xMnO_3$ (x = 0.0, 0.2, 0.3, 0.4, 0.5) compounds, several magnetic isotherms were taken. The magnetic entropy change was calculated by using the well-known Maxwell thermodynamic relation:

$$\Delta S = \int_0^H (\partial M/\partial T)\mathrm{d}H. \quad (2)$$

Generally, for antiferromagnetic systems, the $-\Delta S(T)$ curve shows a positive to negative crossover and a peak is observed for ferromagnetic systems. In our study, a large magnetocaloric effect is observed for all the compounds in the cryogenic temperature range (Fig. 7(a–e)). Hence, they may be suitable candidates for refrigerant materials. Fig. 7(a) shows that the maximum value of entropy change for the GSMO compound is nearly 10.15 J kg^{-1} K^{-1} and a peak is observed at T = 7.5 K. With increasing the doping concentration of Ca (replacing Sr), the value of the magnetic entropy change also increases. Although the increases of $-\Delta S(T)$ for the x = 0.2, 0.3, 0.4 compounds are

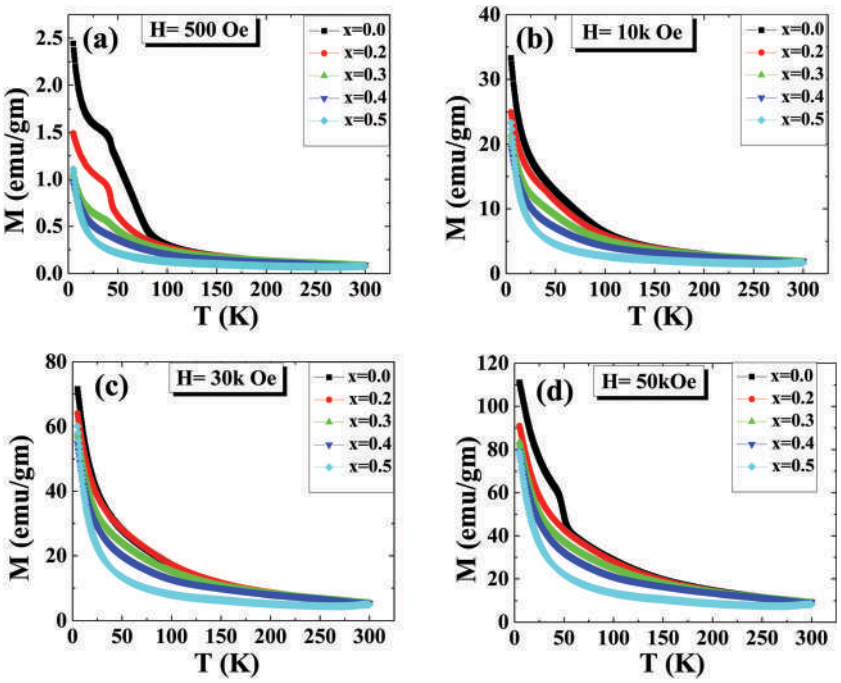

Fig. 5 Temperature dependent magnetization for $Gd_{0.5}Sr_{0.5-x}Ca_xMnO_3$ (x = 0.0, 0.2, 0.3, 0.4, 0.5) compounds at (a) H = 500 Oe, (b) H = 10 kOe, (c) H = 30 kOe and (d) H = 50 kOe external magnetic field.

Published on 23 March 2022. Downloaded by Indian Institute of Technology Kanpur on 4/11/2022 7:21:08 AM.

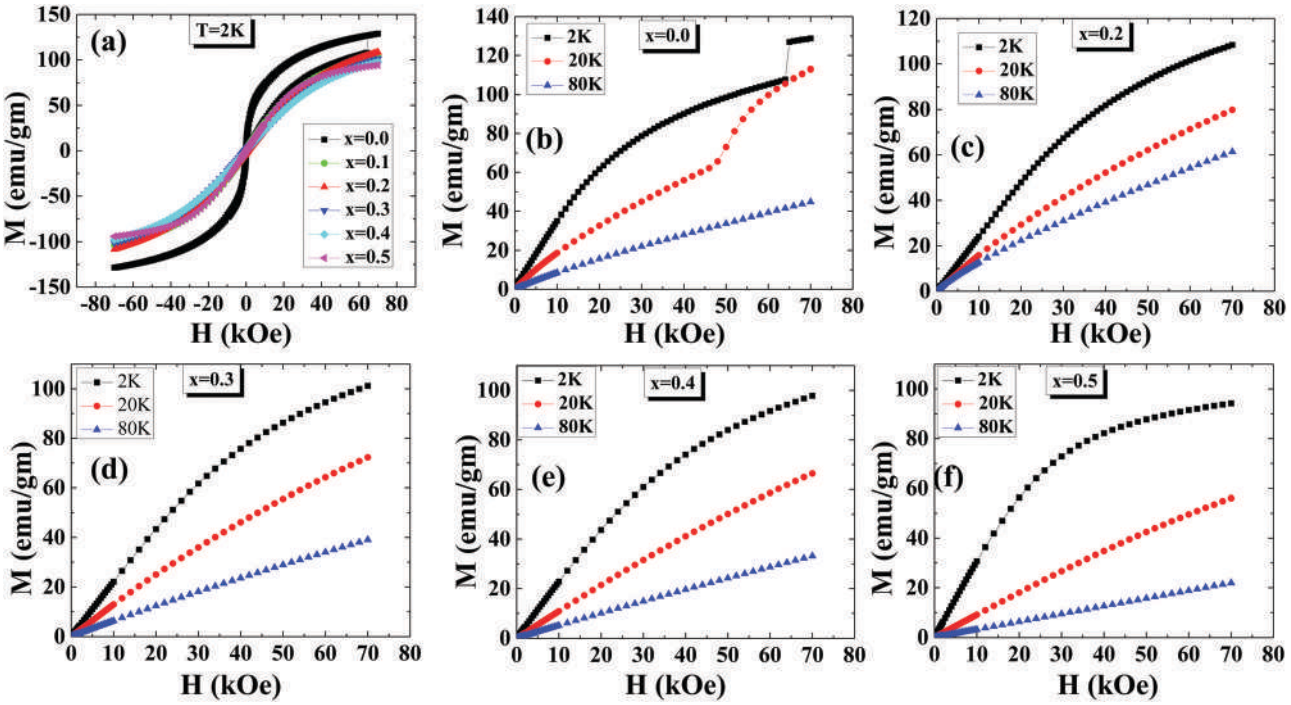

Fig. 6 Magnetization as a function of the magnetic field for the $Gd_{0.5}Sr_{0.5-x}Ca_xMnO_3$ compounds (a) at T = 2 K for x = 0.0, 0.2, 0.3, 0.4, 0.5 and at T = 2 K, 20 K and 80 K for (b) x = 0.0, (c) x = 0.2, (d) x = 0.3, (e) x = 0.4 and (f) x = 0.5.

not so large, for the GCMO compound, a much larger value of MCE is observed. The x = 0.0, 0.2, 0.3 compounds show a peak value of magnetic entropy change at T = 2 K, which may be associated with a glassy transition (disordered ferromagnetic). This peak almost disappears for the x = 0.4 and totally disappears for the x = 0.5 compounds. The absence of a glassy

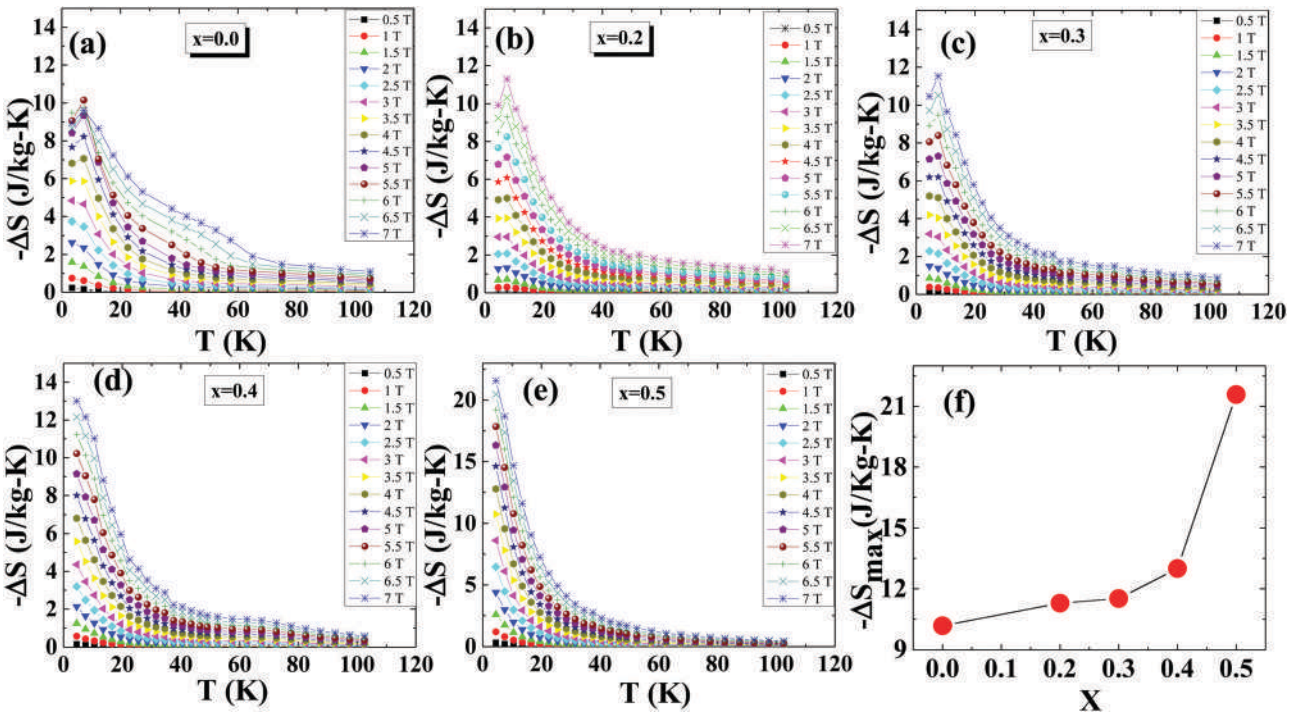

Fig. 7 Variation of magnetic entropy change with temperature for the $Gd_{0.5}Sr_{0.5-x}Ca_xMnO_3$ compounds at several different magnetic fields with (a) x = 0.0, (b) x = 0.2, (c) x = 0.3, (d) x = 0.4 and (e) x = 0.5, and (f) presents the variation of the maximum value of the magnetic entropy change with the doping concentration x for the $Gd_{0.5}Sr_{0.5-x}Ca_xMnO_3$ (x = 0.0, 0.2, 0.3, 0.4 and 0.5) compounds.

 This journal is © the Owner Societies 2022

Published on 23 March 2022. Downloaded by Indian Institute of Technology Kanpur on 4/11/2022 7:21:08 AM.

transition for the GCMO compound is also confirmed by the magnetocaloric curve (Fig. 7(e)). The variation of the maximum entropy change with the doping concentration (x) is shown in Fig. 7(f).

It is important to note that, in the paramagnetic region ($T > 100$ K), the width of the $-\Delta S(T)$ curve at different constant magnetic fields decreased from $x = 0.0$ to $x = 0.5$. Although in the cryogenic temperature region, $-\Delta S(T)$ is smaller for the GSMO compound, in the paramagnetic region, it is larger for GSMO than the other compounds. Generally, the specimens with large magnetization show large values of the magnetocaloric effect (MCE), but our experimental results show that a large MCE corresponds to a smaller magnetization value. Here, the GSMO compound with a large magnetization value gives a smaller magnetocaloric effect and the GCMO compound with smaller magnetization displays a large magnetocaloric effect (Fig. 2(f) and 7(f)). Hence, it may be argued that the large value of the MCE is influenced not only by the magnetization values but also by the strength and nature of the interaction. Aside from those reasons, in our present study, such an anomalous nature of the magnetocaloric effect may also be associated with the anomalous structural change in the GCMO compound.

To get more insights, we have compared the nature of the magnetocaloric effect and magnetization for our studied samples in the paramagnetic region. The variation of magnetization and $-\Delta S$ with the doping concentration x is shown in Fig. 8(a and b) respectively. Fig. 8(a and b) indicate that in the paramagnetic region, the $-\Delta S(x)$ and magnetization curves follow the same nature (in the paramagnetic region there is no interaction).

Rodriguez-Martinz *et al.* have already reported that the magnetic and electronic properties of manganite depend on the tolerance factor (t), as well as the variance (σ^2).[68] t is related to the transfer integral (b) and σ^2 is associated with the random distribution of Mn–O–Mn bond angles. We have listed the values of t and σ^2 for the $Gd_{0.5}Sr_{0.5-x}Ca_xMnO_3$ (x = 0.0, 0.2, 0.3, 0.4, 0.5) compounds in Table 4 (considering $r_{Gd^{3+}}$ = 107.8 pm, $r_{Ca^{2+}}$ = 114 pm, $r_{Sr^{2+}}$ = 132pm, $r_{Mn^{3+}}$ = 72 pm, $r_{Mn^{4+}}$ = 67 pm and $r_{O^{2-}}$ = 126 pm). According to Shannon's work,[69] the ionic radius depends on the coordination number (CN). So, the tolerance factor t is also dependent on CN.

Table 4 Tolerance factors (t) and variance (σ^2) for the $Gd_{0.5}Sr_{0.5-x}Ca_xMnO_3$ (x = 0.0, 0.2, 0.3, 0.4 and 0.5) compounds

Compound	t	σ^2 (pm^2)
$Gd_{0.5}Sr_{0.5}MnO_3$	0.890	146
$Gd_{0.5}Sr_{0.3}Ca_{0.2}MnO_3$	0.877	110.71
$Gd_{0.5}Sr_{0.2}Ca_{0.3}MnO_3$	0.871	83.77
$Gd_{0.5}Sr_{0.1}Ca_{0.4}MnO_3$	0.864	49.93
$Gd_{0.5}Ca_{0.5}MnO_3$	0.858	9.61

Here, CN = 6 is used for all the ions (Sr^{2+}, Ca^{2+}, Gd^{3+}, Mn^{3+} and Mn^{4+}) to determine the tolerance factors of all the compounds.[69]

The values in Table 4 indicate that the tolerance factors of all the compounds are in the same order of magnitude but the value of σ^2 is much larger for GSMO than the GCMO compound. The exact values of the tolerance factors show that t is larger for GSMO and gradually decreases up to GCMO. Upon decreasing the tolerance factor (t), both the Mn–O–Mn bond angle and transfer integral (b) decrease and the e_g electrons tend to hop from the itinerant state to the localized state. So, the charge-ordered transition temperature (T_{CO}) increases with a decreasing tolerance factor.[64] Our present study also shows that for the GCMO compound (smaller t), the T_{CO} is greater than that of the GSMO compound (larger t).

A large value of σ^2 is closely related to the transfer integral (b). The magnetically and electrically inhomogeneous nature of a specimen can be detected from the randomness of the transfer integral (b). Teresa *et al.* have already reported that depending on the value of b, the specimen consists with ferromagnetic and antiferromagnetic regions.[70] Terai *et al.* suggests that this behavior is a spin glass state.[64]

So, materials with a large value of σ^2 can show a spin glass state. In our experimental study, the GSMO compound (having a large σ^2) shows glassy behavior and upon increasing the doping concentration (x), σ^2 decreases. So, the glassiness of the compounds also decreases gradually and for the GCMO compound this glassy behavior disappears. The variation of σ^2 with the tolerance factor is shown in Fig. 8(c).

The appearance of the exchange bias and training effect are very well studied phenomena in phase separated magnetic

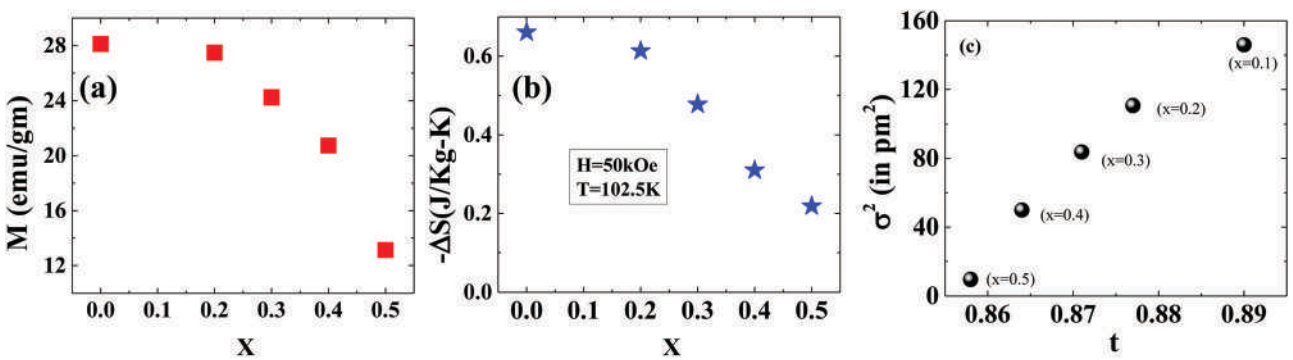

Fig. 8 Variation of (a) magnetization in the paramagnetic region (T = 102.5 K and H = 50 kOe) and (b) magnetic entropy change at T = 102.5 K and H = 50 kOe with the Ca doping concentration (x). (c) The variation of variance (σ^2) with the tolerance factor (t) for the series of $Gd_{0.5}Sr_{0.5-x}Ca_xMnO_3$ (x = 0.0, 0.2, 0.3, 0.4, 0.5) compounds.

Published on 23 March 2022. Downloaded by Indian Institute of Technology Kanpur on 4/11/2022 7:21:08 AM.

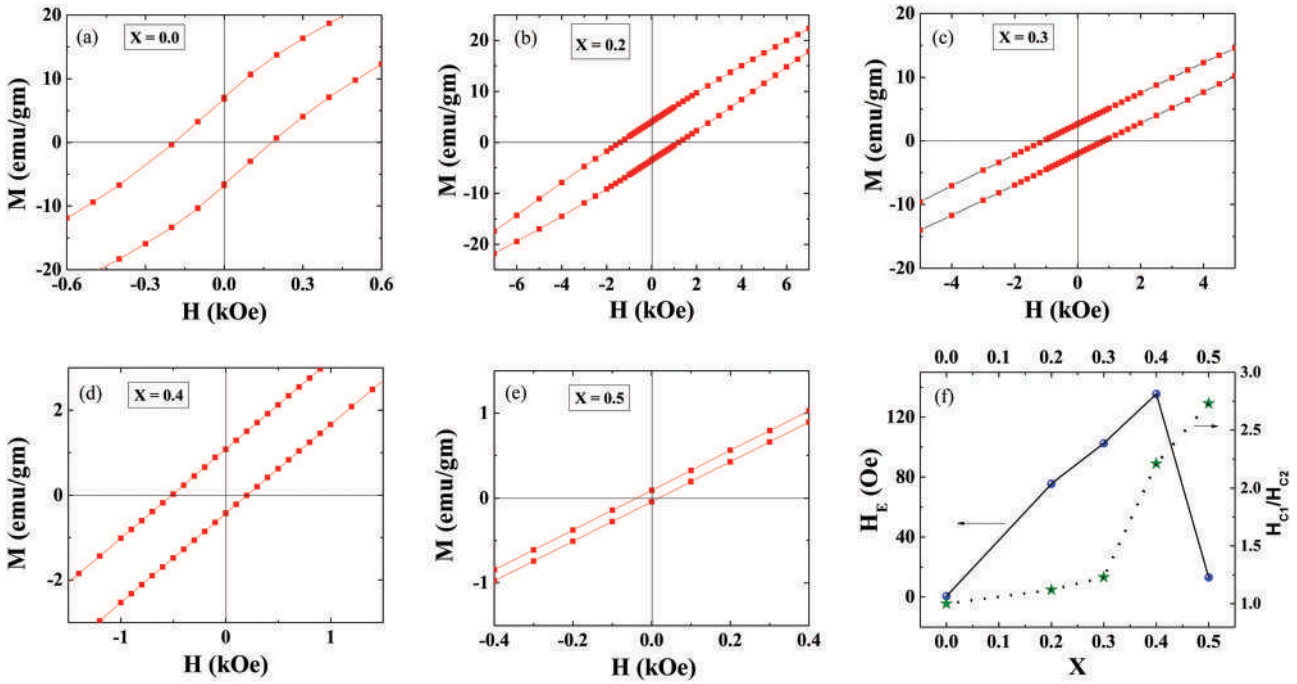

Fig. 9 (a–e) Enlarged view of the magnetization as a function of the magnetic field at 2 K after the cooling down of the sample in the presence of a 70 kOe magnetic field from the paramagnetic state (T = 300 K). (f) Variation of the exchange bias field and asymmetry (ratio of negative and positive coercive fields) of the $Gd_{0.5}Sr_{0.5-x}Ca_xMnO_3$ (x = 0.0, 0.2, 0.3, 0.4, 0.5) compounds with doping concentration x.

materials.[71] The unidirectional spin pinning arises due to the cooling down of the sample in the presence of an external magnetic field, known as the exchange bias effect. This is quantified by the expression

$$H_E = \frac{H_{C1} - H_{C2}}{2}, \quad (3)$$

where H_{C1} and H_{C2} denote the magnitude of the left and right coercivity fields respectively. In our studied sample, the exchange bias phenomenon at T = 2 K (due to the cooling field 70 kOe) is shown in Fig. 9(a–e). Interestingly, the effect of the phase coexisting nature is reflected in our present study (shown in Fig. 9(f)). As the magnetic phases are quite stable for the x = 0.0 and x = 0.5 compounds, the exchange bias is reduced compared to those of the intermediate doped samples. However, the relative change of the coercivity (H_{C1}/H_{C2}) is highest for the x = 0.5 compound, possibly due to charge order stability, as reported previously.[71] Regarding this context, it is worth mentioning that the width of the hysteresis loop decreases with the doping concentration x in the $Gd_{0.5}Sr_{0.5-x}Ca_xMnO_3$ compounds. Such an effect is directly correlated with the ordering nature of the compounds. For the GSMO compound, a field induced first order to second order nature transition is observed from the Arott plot. In contrast to this, for GCMO, only second order nature is visible for the whole of the measured field range. The magnetocaloric effect increases with the doping concentration x (which corresponds to the decrease of the hysteresis width). The decreasing nature of the magnetic hysteresis loop due to field cycling indicates the superiority of the magnetic refrigerants with higher Ca doping concentrations.

4 Conclusions

To summarize, the influence of the competing nature of glassy and canted magnetic phases on the magnetic, magnetocaloric and exchange bias effects has been explained for polycrystalline $Gd_{0.5}Sr_{0.5-x}Ca_xMnO_3$ (x = 0.0, 0.2, 0.3, 0.4, 0.5) compounds. The estimated magnetocaloric entropy change is drastically modified with the doping concentration x. Interestingly, in contrast to previously reported studies, we have observed the distinct nature of the quantitative values of the magnetocaloric entropy change and magnetization, especially at the low temperature region. A similar nature also appeared in the case of the exchange bias studies. Such distinct features were addressed by considering the modification of the magnetic interactions for different doping concentrations.

Author contributions

K. D., I. D., and S. C. developed the concept of study. S. C. prepared the samples and performed all experimental work. All authors contributed to the manuscript preparation.

Conflicts of interest

There are no conflicts of interest to declare.

Acknowledgements

The work was supported by the Department of Atomic Energy (DAE), Govt. of India. We are grateful to S. Kumar, R. Mondal, and N. Mondal for FESEM measurements.

 This journal is © the Owner Societies 2022

Published on 23 March 2022. Downloaded by Indian Institute of Technology Kanpur on 4/11/2022 7:21:08 AM.

References

1 A. Biswas, T. Samanta, S. Banerjee and I. Das, *J. Appl. Phys.*, 2008, **103**, 013912.
2 A. Biswas, S. Chandra, T. Samanta, M. H. Phan, I. Das and H. Srikanth, *J. Appl. Phys.*, 2013, **113**, 17A902.
3 H. B. Hamed, M. Hoffmann, W. A. Adeagbo, A. Ernst and W. Hergert, *Phys. Status Solidi B*, 2020, **257**, 1900632.
4 A. A. Wagh, K. G. Suresh, P. S. A. Kumar and S. Elizabeth, *J. Phys. D: Appl. Phys.*, 2015, **48**, 135001.
5 T. Kimura, G. Lawes, T. Goto, Y. Tokura and A. P. Ramirez, *Phys. Rev. B: Condens. Matter Mater. Phys.*, 2005, **71**, 224425.
6 J. L. Cohn, M. Peterca and J. J. Neumeier, *Phys. Rev. B: Condens. Matter Mater. Phys.*, 2004, **70**, 214433.
7 A. Biswas and I. Das, *Phys. Rev. B: Condens. Matter Mater. Phys.*, 2006, **74**, 172405.
8 S. Chandra, A. I. Figueroa, B. Ghosh, M. H. Phan, H. Srikanth and A. K. Raychaudhuri, *J. Appl. Phys.*, 2011, **109**, 07D720.
9 Z. B. Guo, Y. W. Du, J. S. Zhu, H. Huang, W. P. Ding and D. Feng, *Phys. Rev. Lett.*, 1997, **78**, 1142.
10 Z. B. Guo, J. R. Zhang, H. Huang, W. P. Ding and Y. W. Du, *Appl. Phys. Lett.*, 1997, **70**, 904.
11 M. H. Phan and S. C. Yu, *J. Magn. Magn. Mater.*, 2007, **308**, 325.
12 S. Jin, T. H. Tiefel, M. McCormack, R. A. Fastnacht, R. Ramesh and L. H. Chen, *Science*, 1994, **264**, 413.
13 M. H. Phan, M. B. Morales, N. S. Bingham, H. Srikanth, C. L. Zhang and S. W. Cheong, *Phys. Rev. B: Condens. Matter Mater. Phys.*, 2010, **81**, 094413.
14 Y. Tokura, *Colossal Magnetoresistive Oxides*, Gordon and Breach Science Publishers, The Netherlands, 2000.
15 H. Kuwahara, Y. Tomioka, A. Asamitsu, Y. Moriotomo and Y. Tokura, *Science*, 1995, **270**, 961.
16 A. Biswas, T. Samanta, S. Banerjee and I. Das, *Appl. Phys. Lett.*, 2008, **92**, 012502.
17 Y. Tokura, *Rep. Prog. Phys.*, 2006, **69**, 797.
18 S. Dong, F. Gao, Z. Q. Wang, J. M. Liu and Z. F. Ren, *Appl. Phys. Lett.*, 2007, **90**, 082508.
19 S. Dong, R. Yu, S. Yunoki, J. M. Liu and E. Dagotto, *Phys. Rev. B: Condens. Matter Mater. Phys.*, 2008, **78**, 064414.
20 R. Rawat, P. Chaddah, P. Bag, K. Das and I. Das, *J. Phys.: Condens. Matter*, 2012, **24**, 416001.
21 A. Banerjee, Kranti Kumar and P. Chaddah, *J. Phys.: Condens. Matter*, 2009, **21**, 026002.
22 Y. Tomioka, A. Asamitsu, H. Kuwahara, Y. Moritomo and Y. Tokura, *Phys. Rev. B: Condens. Matter Mater. Phys.*, 1996, **53**, R1689.
23 Y. Okimoto, Y. Tomioka, Y. Onose, Y. Otsuka and Y. Tokura, *Phys. Rev. B:Condens. Matter Mater. Phys.*, 1998, **57**, R9377.
24 K. Das, B. Satpati and I. Das, *RSC Adv.*, 2015, **5**, 27338.
25 K. Das, R. Rawat, B. Satpati and I. Das, *Appl. Phys. Lett.*, 2013, **103**, 202406.
26 S. Lee, H. Y. Hwang, B. I. Shraiman, W. D. Ratcliff and S. W. Cheong, *Phys. Rev. Lett.*, 1999, **82**, 4508.
27 L. Pi, J. Cai, Q. Zhang, S. Tan and Y. Zhang, *Phys. Rev. B: Condens. Matter Mater. Phys.*, 2005, **71**, 134418.
28 K. R. Mavani and P. L. Paulose, *Europhys. Lett.*, 2007, **78**, 37004.
29 N. S. Bingham, P. Lampen, M. H. Phan, T. D. Hoang, H. D. Chinh, C. L. Zhang, S. W. Cheong and H. Srikanth, *Phys. Rev. B: Condens. Matter Mater. Phys.*, 2012, **86**, 064420.
30 P. Lampen, A. Puri, M. H. Phan and H. Srikanth, *J. Alloys Compd.*, 2012, **512**, 94–99.
31 P. Lampen, N. S. Bingham, M. H. Phan, H. Kim, M. Osofsky, A. Pique, T. L. Phan, S. C. Yu and H. Srikanth, *Appl. Phys. Lett.*, 2013, **102**, 062414.
32 M. H. Phan, S. Chandra, N. S. Bingham, H. Srikanth, C. L. Zhang, S. W. Cheong, T. D. Hoang and H. D. Chinh, *Appl. Phys. Lett.*, 2010, **97**, 242506.
33 N. I. Kourov, V. G. Pushin, A. V. Korolev, V. V. Marchenkov, E. B. Marchenkova, V. A. Kazantsev, N. N. Kuranova and A. G. Popov, *Phys. Solid State*, 2013, **55**, 2471–2478.
34 X. F. Wang, Y. J. Yan, J. J. Ying, Q. J. Li, M. Zhang, N. Xu and X. H. Chen, *J. Phys.: Condens. Matter*, 2010, **22**, 075702.
35 K. Das, P. Dasgupta, A. Poddar and I. Das, *Sci. Rep.*, 2016, **6**, 20351.
36 E. R. Buzin, W. Prellier, B. Mercey, C. Simon and B. Raveau, *J. Phys.: Condens. Matter*, 2002, **14**, 3951–3958.
37 W. Prellier, E. R. Buzin, C. Simon, B. Mercey, M. Hervieu, S. de Brion and G. Chouteau, *Phys. Rev. B: Condens. Matter Mater. Phys.*, 2002, **66**, 024432.
38 E. R. Buzin, W. Prellier, C. Simon, S. Mercone, B. Mercey, B. Raveau, J. Sebek and J. Hejtmanek, *Appl. Phys. Lett.*, 2001, **79**, 5.
39 A. M. Tishin and Y. I. Spichkin, *The Magnetocaloric Effect and its Applications*, Institute of Physics Publishing, Bristol and Philadelphia, 2003.
40 T. Samanta, A. U. Saleheen, D. L. Lepkowski, A. Shankar, I. Dubenko, A. Quetz, M. Khan, N. Ali and S. Stadler, *Phys. Rev. B: Condens. Matter Mater. Phys.*, 2014, **90**, 064412.
41 K. Das and I. Das, *J. Appl. Phys.*, 2016, **119**, 093903.
42 K. A. Gschneidner Jr., V. K. Pecharsky and A. O. Tsokol, *Rep. Prog. Phys.*, 2005, **68**, 1479–1539.
43 A. O. Pecharsky, K. A. Gschneidner Jr. and V. K. Pecharsky, *J. Appl. Phys.*, 2003, **93**, 4722–4728.
44 O. Tegus, E. Bruck, K. H. J. Buschow and F. R. deBoerd, *Nature*, 2002, **415**, 150–152.
45 H. Wada and Y. Tanabe, *Appl. Phys. Lett.*, 2001, **79**, 3302–3304.
46 H. Wada, Y. Tanabe, M. Shiga, H. Sugawara and H. Sato, *J. Alloys Compd.*, 2001, **316**, 245–249.
47 N. K. Singh, K. G. Suresh, A. K. Nigam and S. K. Malik, *J. Appl. Phys.*, 2005, **97**, 10A301.
48 T. Samanta, I. Das and S. Banerjee, *Appl. Phys. Lett.*, 2007, **91**, 152506.
49 T. Samanta, I. Das and S. Banerjee, *Appl. Phys. Lett.*, 2007, **91**, 082511.
50 K. Das, T. Paramanik and I. Das, *J. Magn. Magn. Mater.*, 2015, **374**, 707–710.
51 K. Das, S. Banik and I. Das, *Mater. Res. Bull.*, 2016, **73**, 256–260.
52 T. Samanta, D. L. Lepkowski, A. U. Saleheen, A. Shankar, J. Prestigiacomo, I. Dubenko, A. Quetz, W. H. Oswald,

Published on 23 March 2022. Downloaded by Indian Institute of Technology Kanpur on 4/11/2022 7:21:08 AM.

G. T. McCandless, J. Y. Chan, P. W. Adams, D. P. Young, N. Ali and S. Stadler, *Phys. Rev. B: Condens. Matter Mater. Phys.*, 2015, **91**, 020401(R).
53 F. Dobrich, J. Kohlbrecher, M. Sharp, H. Eckerlebe, R. Birringer and A. Michels, *Phys. Rev. B: Condens. Matter Mater. Phys.*, 2012, **85**(9), 094411.
54 D. H. Ryan, A. Michels, F. Deobrich, R. Birringer, Z. Yamani and J. M. Cadogan, *Phys. Rev. B: Condens. Matter Mater. Phys.*, 2013, **87**(6), 064408.
55 M. H. Phan and S. C. Yu, *J. Magn. Magn. Mater.*, 2007, **308**, 325–340.
56 T. Samanta, I. Das and S. Banerjee, *Appl. Phys. Lett.*, 2007, **91**, 082511.
57 Q. Y. Dong, B. G. Shen and J. Chen, *J. Appl. Phys.*, 2009, **105**, 07A305.
58 A. A. Wagh, P. S. A. Kumar, H. L. Bhatand and S. Elizabeth, *J. Phys.: Condens. Matter*, 2010, **22**, 026005.
59 A. A. Wagh, P. S. A. Kumar and S. Elizabeth, *Mater. Res. Express*, 2016, **3**, 106102.
60 A. Beiranvand, J. Tikkanen, H. Huhtinen and P. Paturi, *J. Alloys Compd.*, 2017, **720**, 126.
61 A. Ghosh, T. Ahmed, D. A. Yarotski, S. M. Nakhmanson and J. X. Zhu, *EPL*, 2016, **116**, 57002.
62 R. Mnassri and A. Cheikhrouhou, *J. Supercond. Novel Magn.*, 2014, **27**, 1463–1468.
63 H. Taguchi, M. Nagao and M. Shimada, *J. Solid State Chem.*, 1989, **82**, 8–13.
64 T. Terai, T. Sasaki, T. Kakeshita, T. Fukuda, T. Saburi, H. Kitagawa, K. Kindo and M. Honda, *Phys. Rev. B: Condens. Matter Mater. Phys.*, 2000, **61**, 5.
65 R. Tlili, M. Bejar, E. Dhahri, A. Zaoui, E. K. Hlil and L. Bessais, *Polyhedron*, 2017, **121**, 19–24.
66 P. Dasgupta, S. Paul, N. Mondal, S. Kumar, S. Yarlagadda and C. Mazumdar, *Phys. Rev. B*, 2021, **104**, 035132.
67 B. S. Nagaraja, A. Rao, P. D. Babu, G. Sanjeev and G. S. Okram, *Nucl. Instrum. Methods Phys. Res., Sect. B*, 2016, **366**, 188–197.
68 L. M. Rodriguez-Martinez and J. P. Attfield, *Phys. Rev. B: Condens. Matter Mater. Phys.*, 1996, **54**, R15622.
69 R. D. Shannon, *Acta Crystallogr., Sect. A: Cryst. Phys., Diffr., Theor. Gen. Crystallogr.*, 1976, **32**, 751–767.
70 J. M. D. Teresa, M. R. Ibarra, J. Garcia, J. Blasco, C. Ritter, P. A. Algarabel, C. Marquina and A. Moral, *Phys. Rev. Lett.*, 1996, **76**, 3392.
71 P. Dasgupta, K. Das, S. Pakhira, C. Mazumdar, S. Mukherjee, S. Mukherjee and A. Poddar, *Sci. Rep.*, 2017, **7**, 3220.

 This journal is © the Owner Societies 2022